Thin-Film Flow in Open Helically-Wound Channels

Y. M. Stokes[1]**, S. K. Wilson**[2] **and B. R. Duffy**[2]

[1]Applied Mathematics, School of Mathematical Sciences
The University of Adelaide, SA, 5005 AUSTRALIA

[2]Department of Mathematics
University of Strathclyde, Glasgow, G1 1XH UK

Figure 1: A right-handed helically-wound channel.

Abstract

The study of flow in open helically-wound channels has application to many natural and industrial flows, including those in static spiral separators. The flow consists of a primary axial component and a secondary cross flow and, in spiral separators, the fluid depth is typically small making experimental investigation difficult. Mathematical models are therefore of great value for determining how such flows are influenced by fluid properties and geometrical parameters and, hence, for predicting and improving the performance of these separators. A thin-film approximation is appropriate and yields an explicit expression for the fluid velocity in terms of the free-surface shape. The latter satisfies an interesting non-linear ordinary differential equation that can easily be solved numerically and in some cases analytically. The semi-analytic predictions of the thin-film model are found to be in good agreement with much more computationally expensive solutions of the Navier–Stokes equations.

Introduction

Considerable literature exists concerning mathematical modelling of fully-developed flow in *closed* helically-wound pipes [1, 2, 3, 10, 19]. These studies have been motivated by a desire to better understand flows in curved geometries such as arise in many piping systems, and the human blood circulation system in particular. They have shown that, for this type of flow, a steady-state solution can be computed, comprising a velocity component along the axis of the pipe and a secondary cross flow.

Flows in *open* helical channels (figure 1) differ most significantly from their closed-pipe counterparts in having a free surface. They have been studied in the context of river flow and sediment transport [17], distillation of petroleum products [13] and, of particular interest here, spiral particle separation [4, 5, 7, 8, 9, 11, 15, 16]. They are also used in the separation of liquids of different densities (e.g. oil from seawater) or solids and liquids (e.g. in the case of wastewaters) [14].

Spiral particle separators are used in the coal and mineral processing industries to segregate and concentrate particles of different sizes and densities [6, 18]. Considerable advances have been made over the past 40 years in understanding the operation of these and improving their design. Nevertheless, fine mineral separation may yet be further improved with a better understanding of the flow in helical channels [18]. It can also assist with the understanding of flow in more general curved channels, such as occur in rivers and pipe networks that run only partly full.

Experimental studies of helical flows, as in spiral separators, are difficult because of problems with visualisation of the flow [7, 8], so that theoretical and computational fluid dynamics are of great value for predicting performance of new and existing spirals. Experimental work has indicated that the fluid depth is small and that some regions of the flow are not laminar [7].
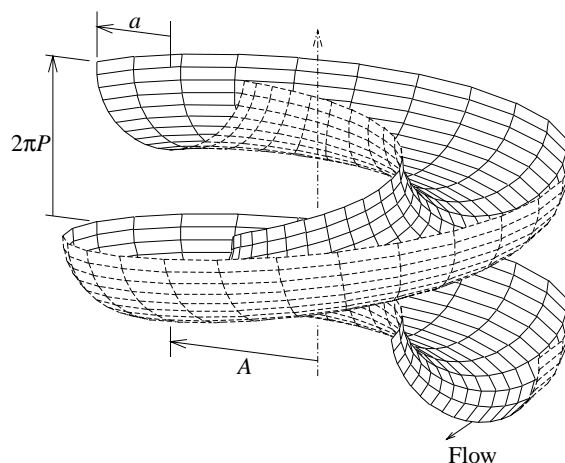
Some CFD simulations have been done [9, 12] but systematic parameter studies to determine how laminar flows in spiral separators are affected by variation of fluid properties and geometrical parameters such as curvature and torsion of the helix, and channel cross-section geometry, have yet to be done. A good understanding of the laminar flow is a necessary precursor to a study of the conditions which lead to turbulence or to the (possibly undesirable) phenomena that develop in the transition to turbulence.

As in [1, 2, 3, 10], we consider laminar flow and seek a steady-state solution that is also independent of axial position. This permits a two-dimensional analysis in the cross-section plane. As part of the solution process, we must determine the free-surface profile of the fluid in the channel, making this analysis significantly different from and more complex than fully developed flows in closed pipes. The shape of the free surface will be primarily determined by the curvature of the helix and the flow rate, so that, at this stage, we ignore surface tension. Since flows in spiral separators are known to be shallow, we concentrate here on thin-film flow. Some consideration to full channels has been given in [15, 16].

Mathematical Model

As in [15, 16] we consider a channel of half-width a, helically wound about a vertical axis with helix radius A and pitch $2\pi P$ (see figure 1). The angle of inclination of the channel to the horizontal is given by $\tan\alpha = P/A$, and the Reynolds and Froude numbers are given by $R = Ua/\nu$, $F = U/\sqrt{ga}$, where U is a characteristic axial flow velocity, ν is the kinematic viscosity of the fluid and g is gravitational acceleration. We also assume small dimensionless curvature $\varepsilon = aA/(A^2 + P^2)$ and sufficiently small torsion ($\tau = \varepsilon \tan\alpha$) such that $R\tau = O(\varepsilon)$, i.e. $R\tan\alpha = O(1)$.
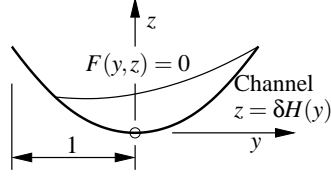
Figure 2: Cross section of channel showing the coordinate system. The *x*-axis is directed out of the page in the direction of the primary axial flow.

We use a Cartesian coordinate system with the *x*-axis in the direction of the primary axial flow and *y* and *z* axes in the cross-section of the channel as shown in figure 2. Lengths are normalised to give a channel half-width of 1. Then, at leading order in ε, the continuity and Navier–Stokes equations give (*cf.* [15, 16])

$$\frac{\partial v}{\partial y} + \frac{\partial w}{\partial z} = 0, \tag{1}$$

$$v\frac{\partial u}{\partial y} + w\frac{\partial u}{\partial z} = \nabla^2 u + \frac{R\sin\alpha}{F^2}, \tag{2}$$

$$v\frac{\partial v}{\partial y} + w\frac{\partial v}{\partial z} - \frac{1}{2}Ku^2 = -\frac{\partial p}{\partial y} + \nabla^2 v, \tag{3}$$

$$v\frac{\partial w}{\partial y} + w\frac{\partial w}{\partial z} = -\frac{\partial p}{\partial z} + \nabla^2 w - \frac{R^2\cos\alpha}{F^2}, \tag{4}$$

where *u* is the primary axial flow velocity (scaled with *U*), *v* and *w* are the secondary flow velocity components (scaled with U/R) in the *y* and *z* directions respectively, *p* is the pressure (scaled with $\rho U^2/R^2$), and $K = 2\varepsilon R^2$ is the Dean number associated with the centrifugal force acting on the flow.

The system (1)–(4) must be solved subject to the conditions for an impermeable, no-slip channel wall, zero stress and the kinematic condition at the free surface, and some prescribed volume flux *Q* down the channel, to give the velocity and pressure distributions in the flow domain and the free-surface shape $F(y,z) = 0$. In practice it is simpler to prescribe the cross-sectional area Ω of the flow domain, rather than the volume flux; then *Q* is computed as an output by integrating $u(y,z)$ over the flow domain, once it has been determined.

In general the solution must be obtained numerically and a method employing finite-element techniques is discussed and demonstrated in [15, 16]. As discussed in those papers, it is necessary to determine the contact points of the free surface with the no-slip wall *a priori* or have a means of adjusting them during the solution process. Here, we use our thin-film solution (discussed below) to obtain first (and very good) estimates of the contact points, and then adjust them iteratively until the required accuracy is achieved.

Thin-Film Approximation

We obtain approximate equations for flows of small depth by defining new variables $z = \delta\tilde{z}$, $v = R\delta\tilde{v}$, $w = R\delta^2\tilde{w}$ and $p = R\tilde{p}/\delta$, where $\delta \ll 1$ is a small aspect ratio. We also choose $\delta^2 R/F^2 = 1$, i.e. velocity scale $U = \delta^2\rho g a^2/\mu$. Substituting into equations (1)–(4) gives, at leading order in δ,

$$\frac{\partial \tilde{v}}{\partial y} + \frac{\partial \tilde{w}}{\partial \tilde{z}} = 0, \tag{5}$$

$$\frac{\partial^2 u}{\partial \tilde{z}^2} + \sin\alpha = 0, \tag{6}$$

$$-\frac{\partial \tilde{p}}{\partial y} + \frac{\partial^2 \tilde{v}}{\partial \tilde{z}^2} + \chi u^2 = 0, \tag{7}$$

$$-\frac{\partial \tilde{p}}{\partial \tilde{z}} - \cos\alpha = 0, \tag{8}$$

where $\chi = \delta K/2R$ is taken to be O(1). Under the thin-film scaling, the boundary conditions on the free surface $F(y,\tilde{z}) = 0$ become

$$\frac{\partial u}{\partial \tilde{z}} = 0, \quad \frac{\partial \tilde{v}}{\partial \tilde{z}} = 0, \quad \tilde{p} = 0 \quad \text{and} \quad \tilde{v}\frac{\partial F}{\partial y} + \tilde{w}\frac{\partial F}{\partial \tilde{z}} = 0.$$

Let the channel shape be given by $\tilde{z} = H(y)$ and the fluid depth be $h(y)$ so that the free surface is at $\tilde{z} = H(y) + h(y)$. Then we may write the solution to the thin-film equations in terms of the functions $H(y)$ and $h(y)$. Thus, integrating (6) and (8), substituting *u* and $\tilde{p}$ into (7) and integrating for $\tilde{v}$ we obtain

$$u = \frac{\sin\alpha}{2}(\tilde{z} - H)(H + 2h - \tilde{z}),$$

$$\tilde{p} = \cos\alpha\,(H + h - \tilde{z}),$$

$$\tilde{v} = -\frac{\chi\sin^2\alpha}{120}(\tilde{z} - H)\times$$
$$\left[(\tilde{z} - H)^3[(H + 2h - \tilde{z})(H + 4h - \tilde{z}) + 2h^2] - 16h^5\right]$$
$$-\frac{\cos\alpha}{2}\frac{\mathrm{d}}{\mathrm{d}y}(H + h)\times(\tilde{z} - H)(H + 2h - \tilde{z}).$$

Writing the continuity equation (5) in the alternative form

$$\int_H^{H+h} \tilde{v}\,d\tilde{z} = 0,$$

substituting for $\tilde{v}$ and integrating yields a first-order ordinary differential equation for *h* for any prescribed channel shape $\tilde{z} = H(y)$:

$$\cos\alpha\,\frac{\mathrm{d}}{\mathrm{d}y}(H + h) = \frac{6\chi\sin^2\alpha}{35}h^4. \tag{9}$$

Defining the stream function ψ such that $\partial\psi/\partial\tilde{z} = \tilde{v}$ and $-\partial\psi/\partial y = \tilde{w}$, substituting for $\tilde{v}$, integrating and requiring $\psi = 0$ on $\tilde{z} = H(y)$ we obtain

$$\psi = \frac{\chi\sin^2\alpha}{840}(\tilde{z} - H)^2(H + 2h - \tilde{z})^2(H + h - \tilde{z})\times$$
$$\left[(H + h - \tilde{z})^2 - 5h^2\right]. \tag{10}$$

The volume flux $Q = \delta\tilde{Q}$ down the channel is given by

$$\tilde{Q} = \int_\ell^r \int_H^{H+h} u\,d\tilde{z}dy = \frac{\sin\alpha}{3}\int_\ell^r h^3\,dy, \tag{11}$$

while the cross-sectional area of the flow domain $\Omega = \delta\tilde{\Omega}$ is given by

$$\tilde{\Omega} = \int_\ell^r h\,dy, \tag{12}$$

where $y = \ell$ and $y = r$ are the left and right ends of the free surface, respectively.

To obtain a thin-film solution for any given channel shape $\tilde{z} = H(y)$ we must solve (9) subject to either (11) or (12) for the fluid depth $h(y)$. Let $h(\ell) = h_\ell$ and $h(r) = h_r$ be the fluid depth at the contact points, i.e. (ℓ, h_ℓ) and (r, h_r) determine the points of contact of the free surface with the channel wall and $\ell \leq y \leq r$. For any channel geometry, two of the four values ℓ, r, h_ℓ, h_r will be known and two must be determined as part of the solution; which two are known depends on the specific channel geometry. In this paper we will consider two different cases, as follows.

1. A rectangular cross section, $H(y) = 0$, $-1 \leq y \leq 1$. In this case the left and right ends of the free surface are on the left and right walls of the channel, so that $\ell = -1$, $r = 1$. However, the fluid depths h_ℓ, h_r are unknown.

2. A parabolic cross section, $H(y) = y^2$. In this case we have zero fluid depth at each end of the free surface, i.e. $h_\ell = h_r = 0$, but the positions $y = \ell, r$ are unknown.

For simple cross sections (such as the rectangular one) we can obtain the thin-film solution analytically, but for more general cross sections (such as the parabolic one) we must solve the thin-film equations numerically, for which we use *Matlab* as follows.

We first guess the unknown value at the left end of the free surface, h_ℓ for the rectangular channel or ℓ for the parabolic channel. Then, (ℓ, h_ℓ) together with (9) defines an initial value problem that is readily solved using the built-in 4th-order Runge-Kutta solver, to give $h(y)$. Finally, we compute the volume flux $\tilde{Q}$ from (11), iteratively adjusting the initial value to give the required flux. Alternatively we may compute the cross-section area $\tilde{\Omega}$ from (12) to adjust the initial value.

Having solved for $h(y)$ we are able to determine the primary axial velocity u and the pressure $\tilde{p}$, and compute streamlines from (10). If desired the cross-flow components $\tilde{v}, \tilde{w}$ may also be calculated.

Comparison of Full Computational and Thin-Film Results

Because of the ease with which we can solve the full Navier–Stokes equations for a specified flow-domain area (and the difficulty in *a priori* prescribing a specified volume flux), it is convenient to compare thin-film solutions and finite-element solutions of the full Navier–Stokes equations for a specified flow domain area $\tilde{\Omega}$ rather than the volume flux $\tilde{Q}$. Thus, we choose the left boundary (ℓ, h_ℓ) for the thin-film solution to give the required area $\tilde{\Omega}$. We then use the thin-film solution $h(y)$, $\ell \leq y \leq r$ as input to our Navier–Stokes model, which we then solve iteratively for the flow velocities, pressure and (modified) free-surface shape. Depending on the desired accuracy this can be a time-consuming process.

The difference in the volume flux $\tilde{Q}$ between the thin-film and Navier–Stokes models gives one (global) measure of comparison. In addition, we may compare contour plots of pressure p, primary axial velocity u, and so on, from each model. Comparing the cross-flow streamlines $\psi = $ constant is particularly informative.

Solutions for both rectangular and parabolic channels have been obtained with a flow domain area $\tilde{\Omega} = 2$ and aspect ratio $\delta = 0.1$. For the thin-film model we already have $\delta^2 R/F^2 = 1$ and we now choose

$$\frac{\chi \sin^2 \alpha}{\cos \alpha} = 1.$$

For the Navier–Stokes model, if we take $\tan \alpha = 4/3$, then we must have

$$\frac{R \sin \alpha}{F^2} = \frac{\sin \alpha}{\delta^2} = 80,$$

and we further choose

$$\frac{R^2 \cos \alpha}{F^2} = \frac{R \cos \alpha}{\delta^2} = 1200.$$

Together, these imply that $R = 20$ and $K = 375$.

The cross-flow streamlines and free surface for the rectangular channel for both thin-film and Navier–Stokes models are plotted in figure 3. The volume flux given by the thin-film model is
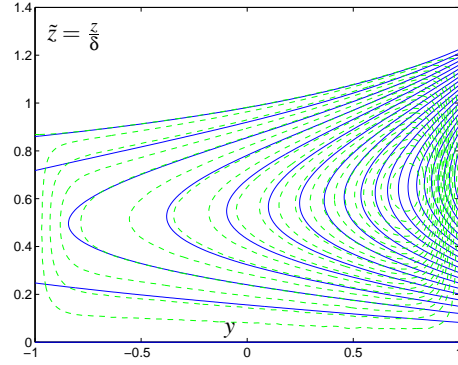
Figure 3: Streamlines of the cross flow in the rectangular channel. Blue (solid) curves correspond to the thin-film model and green (dashed) curves correspond to the Navier–Stokes model.
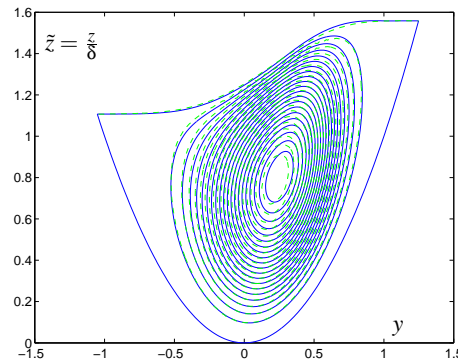
Figure 4: Streamlines of the cross flow in the parabolic channel. Blue (solid) curves correspond to the thin-film model and green (dashed) curves correspond to the Navier–Stokes model.

$\tilde{Q} = 0.55$, while the Navier–Stokes model gives $\tilde{Q} = 0.51$. The differences in the two solutions are primarily due to the vertical side-wall channel boundaries, which are not captured by the present simple thin-film model. In reality there is a thin boundary layer along these walls which the thin-film solution does not show, but which is shown in the solution to the Navier–Stokes model. The thickness of these boundary layers reduces with the aspect ratio δ, and in the thin limit approaches zero thickness. Hence the smaller the value of δ used for our Navier–Stokes solution, the better the agreement with the thin-film solution. The effect of this boundary layer is greater at the wall on the outside of the channel curve, where velocities are greatest, than at the wall on the inside of the curve, where velocities are much smaller. For the case shown ($\delta = 0.1$) we note that, despite the difference between the two models shown by the streamlines, the free-surface shape is quite similar over 85% of its length. Only near the wall at the outside of the channel curve is there any substantial difference.

For smooth channel cross sections (such as the parabolic one) both models incorporate the impermeable, no-slip boundary conditions over the entire channel wall, so we expect to see better agreement between them in this case. The agreement is indeed very good, as shown in figure 4 where the cross-flow streamlines and free surface for both models are plotted. The free-surface shape differs only slightly between the two models, and the streamlines are also quite similar. The thin-film model gives a volume flux of $\tilde{Q} = 0.62$ and the Navier–Stokes model gives $\tilde{Q} = 0.61$, again showing good agreement.

Conclusions

Flow in helically-wound channels of small curvature is governed by the Navier–Stokes equations with an extra term representing the centrifugal force. These equations must, in general, be solved numerically. In some practical applications the flows in such channels are shallow for which a thin-film approximation is appropriate. We have derived a thin-film model and shown that the flow solution can be written in terms of the free-surface shape and the prescribed channel geometry. The free-surface shape is given by a non-linear ordinary differential equation. Solutions are readily obtained for a wide range of channel geometries.

Comparison of results from the Navier–Stokes and thin-film models for rectangular and parabolic channels have been obtained. For the rectangular channel, which has vertical wall boundaries that are handled differently by the two models, the general character of the flow solutions is similar, but they differ near these boundaries, most significantly near the wall on the outside curve of the channel. However, for a channel with a smooth cross section (such as the parabolic one) the two models effectively impose the same boundary conditions and the solutions are in close agreement. For the parabolic channel the thin-film model gives a solution of excellent accuracy at a fraction of the computational effort required to solve the Navier–Stokes equations. This leads us to believe that our thin-film model has excellent potential to provide valuable information on practical open-channel flows (such as occur in spiral separators) both quickly and cheaply. Work is being continued to determine the parameter range over which our thin-film model is valid.

Acknowledgements

References

[1] Berger, S.A., Talbot, L. and Yao, L.-S., Flow in curved pipes, *Ann. Rev. Fluid Mech.*, **15**, 1983, 461–512.

[2] Germano, M., On the effect of torsion on a helical pipe flow, *J. Fluid Mech.*, **125**, 1982, 1–8.

[3] Germano, M., The Dean equations extended to a helical pipe flow, *J. Fluid Mech.*, **203**, 1989, 289–305.

[4] Holland-Batt, A.B., Spiral separation: theory and simulation, *Trans. Instn Min. Metall. (Sect C: Mineral Process. Extr. Metall.)*, **98**, 1989, C45–C60.

[5] Holland-Batt, A.B. and Holtham, P.N., Particle and fluid motion on spiral separators, *Min. Eng.*, **4**, 1991, 457–482.

[6] Holtham, P.N. and Stitt, P.H., Developments in Australian spiral separator technology, *Minerals and Exploration at the Cross Roads, Aus. IMM Annual Conf.*, Sydney, 1988, p. 165.

[7] Holtham, P.N., Flow visualisation of secondary currents on spiral separators, *Min. Eng.*, **3**, 1990, 279–286.

[8] Holtham, P.N., Primary and secondary fluid velocities on spiral separators, *Min. Eng.*, **5**, 1992, 79–91.

[9] Jancar, T., Fletcher, C.A.J., Holtham, P.N. and Reizes, J.A., Computational and experimental investigation of spiral separator hydrodynamics, *Proc. XIX Int. Mineral Proc. Congress*, San Francisco, 1995, 147–151.

[10] Kao, H.C., Torsion effect on fully developed flow in a helical pipe, *J. Fluid Mech.*, **184**, 1987, 335–356.

[11] Matthews, B.W., Fletcher, C.A.J., Partridge, A.C. and Jancar, T., Computational simulation of spiral concentrator flows in the mineral processing industry, *Chemeca '96*.

[12] Matthews, B.W., Fletcher, C.A.J. and Partridge, A.C., Computational simulation of fluid and dilute particulate flows on spiral concentrators, *Inter. Conf. on CFD in Mineral & Metal Processing and Power Generation*, CSIRO, 1997, 101–109.

[13] Morton, F., King, P.J. and McLaughlin, A., Helical-coil distillation columns Part I: Efficiency studies, *Trans. Instn Chem. Engrs*, **42**, 1964, T285–T295.

[14] NASA Patent No 5 248 421, Spiral fluid separator, Marshall Space Flight Center, Technology Transfer Program.

[15] Stokes, Y.M., Flow in spiral channels of small curvature and torsion, in *IUTAM Symposium on Free Surface Flows, Proceedings of the IUTAM Symposium*, Birmingham, United Kingdom, 10–14 July 2000, editors A.C. King and Y.D. Shikhmurzaev, Kluwer, 2001, 289–296.

[16] Stokes, Y.M., Computing flow in a spiral particle separator, *Proceedings of the 14th Australasian Fluid Mechanics Conference*, Adelaide University, Australia, 9–14 December 2001, 677–680.

[17] Thomson, J., On the origin of windings of rivers in alluvial plains, with remarks on the flow of water round bends in pipes, *Proc. R. Soc. Lond. Ser. A*, **5**, 1876, 5–8.

[18] Weldon, B., Fine Coal Beneficiation: Spiral separators in the Australian industry, *The Australian Coal Review*, Nov. 1997, 25–28.

[19] Zabielski, L. and Mestel, A.J., Steady flow in a helically symmetric pipe, *J. Fluid Mech.*, **370**, 1998, 297–320.